ACS Chemical Biology

Articles

Cite This: ACS Chem. Biol. 2019, 14, 2315−2326

pubs.acs.org/acschemicalbiology

Double Monoubiquitination Modifies the Molecular Recognition Properties of p15^{PAF} Promoting Binding to the Reader Module of Dnmt1

Amaia González-Magaña,[†] Alain Ibáñez de Opakua,[†] Nekane Merino,[†] Hugo Monteiro,[‡] Tammo Diercks,[†] Javier Murciano-Calles,[§] Irene Luque,[§] Pau Bernadó,[∥] Tiago N. Cordeiro,[‡] Alfredo De Biasio,[⊥] and Francisco J. Blanco*[,†,#]

[†]CIC bioGUNE, 48160 Derio, Spain

[‡]Instituto de Tecnologia Química e Biológica António Xabier, ITQB NOVA, 2780-157 Oeiras, Portugal

[§]Department of Physical Chemistry and Institute of Biotechnology, Universidad de Granada, Granada 18071, Spain

[∥]Centre de Biochimie Structurale, INSERM, CNRS, and Université Montpellier, 34090 Montpellier, France

[⊥]Leicester Institute of Structural & Chemical Biology and Department of Molecular & Cell Biology, University of Leicester, Leicester LE1 7RH, U.K.

[#]IKERBASQUE, Basque Foundation for Science, 48013 Bilbao, Spain

Supporting Information

ABSTRACT: The proliferating cell nuclear antigen (PCNA)-associated factor p15^{PAF} is a nuclear protein that acts as a regulator of DNA repair during DNA replication. The p15^{PAF} gene is overexpressed in several types of human cancer, and its function is regulated by monoubiquitination of two lysines (K15 and K24) at the protein N-terminal region. We have previously shown that p15^{PAF} is an intrinsically disordered protein which partially folds upon binding to PCNA and independently contacts DNA through its N-terminal tail. Here we present an NMR conformational characterization of p15^{PAF} monoubiquitinated at both K15 and K24 via a disulfide bridge mimicking the isopeptide bond. We show that doubly monoubiquitinated p15^{PAF} is monomeric, intrinsically disordered, and binds to PCNA as nonubiquitinated p15^{PAF} does but interacts with DNA with reduced affinity. Our SAXS-derived conformational ensemble of doubly monoubiquitinated p15^{PAF} shows that the ubiquitin moieties, separated by eight disordered residues, form transient dimers because of the high local effective ubiquitin concentration. This observation and the sequence similarity with histone H3 N-terminal tail suggest that doubly monoubiquitinated p15^{PAF} is a binding target of DNA methyl transferase Dnmt1, as confirmed by calorimetry. Therefore, doubly monoubiquitinated p15^{PAF} directly interacts with PCNA and recruits Dnmt1 for maintenance of DNA methylation during replication.

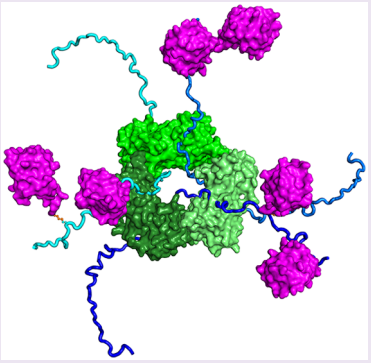

INTRODUCTION

Ubiquitination is a multifunctional post-translational modification that may not only drive the protein through the proteasome degradation pathway, but also change the affinity for binding to other biomolecules and, thus, affect protein function in a variety of cellular processes. A few ubiquitinated proteins have been structurally studied and shown to preserve their three-dimensional structure; however, the impact of this modification may be particularly strong in the case of intrinsically disordered proteins (IDPs), whose conformational equilibrium might be significantly altered.[1] A conformational and molecular recognition characterization of an ubiquitinated IDP is still missing, likely because of the difficulties in obtaining high amounts of the pure modified protein. Here we present a thorough structural analysis of the p15^{PAF} oncogenic protein monoubiquitinated at two lysine residues via a disulfide bridge that mimics the isopeptide bond.

The p15^{PAF} protein (hereafter named p15) is a nuclear 12 kDa polypeptide initially identified as a proliferating cell nuclear antigen (PCNA) binding protein.[2] The DNA sliding clamp PCNA has the shape of a ring and acts as a docking platform for many enzymes that edit DNA.[3] p15 binds to the front face of the PCNA ring as it encircles the DNA and slides along it.[4] Regulatory monoubiquitination at residues K15 and K24 (Figure 1A) selectively occurs on PCNA-bound p15 during the S phase of the cell cycle,[5] when replicative DNA polymerases copy the DNA. The ubiquitination of p15 is mediated by the E3 ligase UHFR1 (ubiquitin-like PHD and RING finger containing domain 1),[6] which also monoubiquitinates the histone H3 N-terminal tail at two sites.[7,8] Following

Received: August 22, 2019
Accepted: September 3, 2019
Published: September 3, 2019

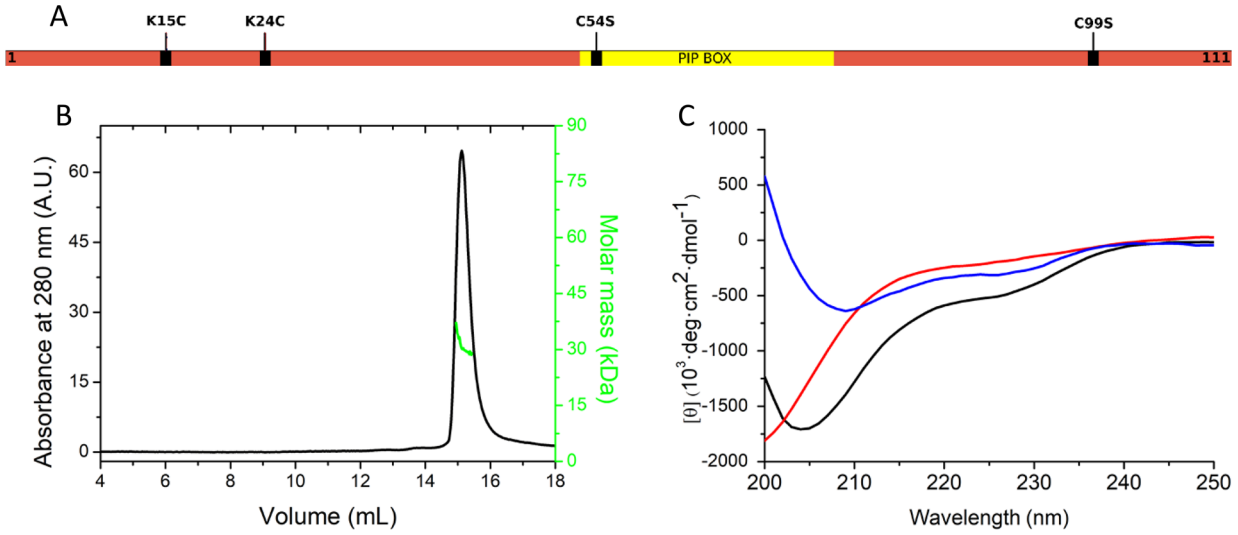

Figure 1. dmUbp15 is monomeric and unstructured in solution. (A) Scheme of p15 showing the position of the mutations introduced in this study (p15CCSS) as well as the PIP-box region (yellow), encompassing all the residues observed in the crystal structure with PCNA.[20] (B) Size exclusion chromatogram of dmUbp15 (black, axis on the left) and molar mass derived from MALS (green, axis on the right) in PBS pH 7.0 at 25 °C. The theoretical molar mass of dmUbp15 is 29 019 Da (Figure S1). (C) CD spectra of dmUbp15 (black), p15CCSS (red), and their difference (blue).

UV stress, the interaction of doubly monoubiquitinated p15 (hereafter named dmUbp15) with PCNA is disrupted, inducing the recruitment of the trans-lesion synthesis (TLS) polymerase η to PCNA at stalled replisomes and, thus, facilitating the bypass of replication-fork blocking lesions.[5] It is thought that, upon DNA-replication blockage, the mono-ubiquitinated sites are polyubiquitinated and p15 is removed from PCNA in a proteasome-dependent manner.[5] p15 is an emergent cancer target as it is overexpressed in multiple types of human cancer and is associated with poor prognosis.[9−11] Recently it has been described as a factor required for the maintenance of breast cancer and glioma cell stemness.[12,13]

The p15 protein is intrinsically disordered in solution[14] but adopts a folded structure for the central region when bound to PCNA.[4] This central region contains the PCNA interacting protein motif (PIP) and tightly binds on the front face of the PCNA ring. In contrast to other PCNA interacting proteins, however, p15 also contacts the inside of, and passes through, the PCNA ring, with the disordered p15 termini emerging at opposite faces of the ring.[4] Both free and PCNA-bound p15 contact DNA mainly with its N-terminal tail, rich in positively charged amino acids, suggesting that p15 acts as a flexible drag to regulate PCNA sliding along the DNA.[4] The distance between the two ubiquitin moieties at the N-terminal region of the p15 sequence and its similarity to the N-terminal tail of histone H3 suggest that dmUbp15 binds the replication foci targeting sequence (RFTS) of DNA methytransferase Dnmt1 as doubly monoubiquitinated histone H3 does.[15]

Here, we present a detailed characterization of the conformational and molecular recognition properties of doubly monoubiquitinated p15. To prepare dmUbqp15, we followed a nonenzymatic approach involving a direct disulfide linkage that mimics the isopeptide bond. The doubly monoubiquitinated protein remains disordered based on circular dichroism (CD), small-angle X-ray scattering (SAXS), and NMR chemical shift data analysis. We show that dmUbp15 binds PCNA and DNA, yet with lower affinity than unmodified p15 in the case of DNA, suggesting a role of p15 in regulating the PCNA sliding velocity on the DNA. Furthermore, dmUbp15 binds the RFTS of Dnmt1 as seen by calorimetry, suggesting that it recruits Dnmt1 to replication forks for maintenance of DNA methylation.

RESULTS

Doubly Monoubiquitinated p15 Remains Intrinsically Disordered. In order to monoubiquitinate p15 at two residues, we used a nonenzymatic approach comprising the introduction of reactive thiol groups both in the ubiquitin and in the target p15 protein.[16,17] The disulfide bond directed ubiquitination yields a sterically similar linkage to the native isopeptide bond.[18] We expressed and purified a p15 mutant with the ubiquitination target lysine residues mutated to cysteine, whereas two native cysteines in the sequence were changed to serine. A reactive ubiquitin added to this p15CCSS mutant spontaneously produced dmUbp15. With this method, we were able to produce milligram amounts of homogeneous dmUbp15 (Figure 1S).

The SEC-MALS analysis of dmUbp15 demonstrated that the protein is a monomer (Figure 1B). The far-UV CD spectrum shows one minimum at 205 nm and a shoulder at 225 nm, consistent with a mixture of random coil and regular secondary structure (Figure 1C). The CD spectrum of the quadruple p15 mutant p15CCSS (used for ubiquitination at positions 15 and 24; see the methods section) is typical for a random coil. The difference spectrum shows the pattern of minima corresponding to the ubiquitin moieties.[19] These results suggest that isolated dmUbp15 lacks any defined structure apart from the ubiquitin moiety.

In contrast to CD and other analytical methods, our studies of dmUbp15 constructs by heteronuclear NMR correlation spectroscopy are selective for the p15 moiety because of its labeling with NMR-active ^{13}C and ^{15}N isotopes, whereas the unlabeled fused ubiquitin moieties remain invisible. The assignment of the p15 backbone and some C^{β} side chain NMR signals was then obtained from a set of conventional triple resonance experiments with out-and-back transfer and detection on the amide protons. The 2D $^{1}H,^{15}N$ HSQC fingerprint spectrum of the p15 moiety in dmUbp15 shows 99

DOI: 10.1021/acschembio.9b00679
ACS Chem. Biol. 2019, 14, 2315−2326

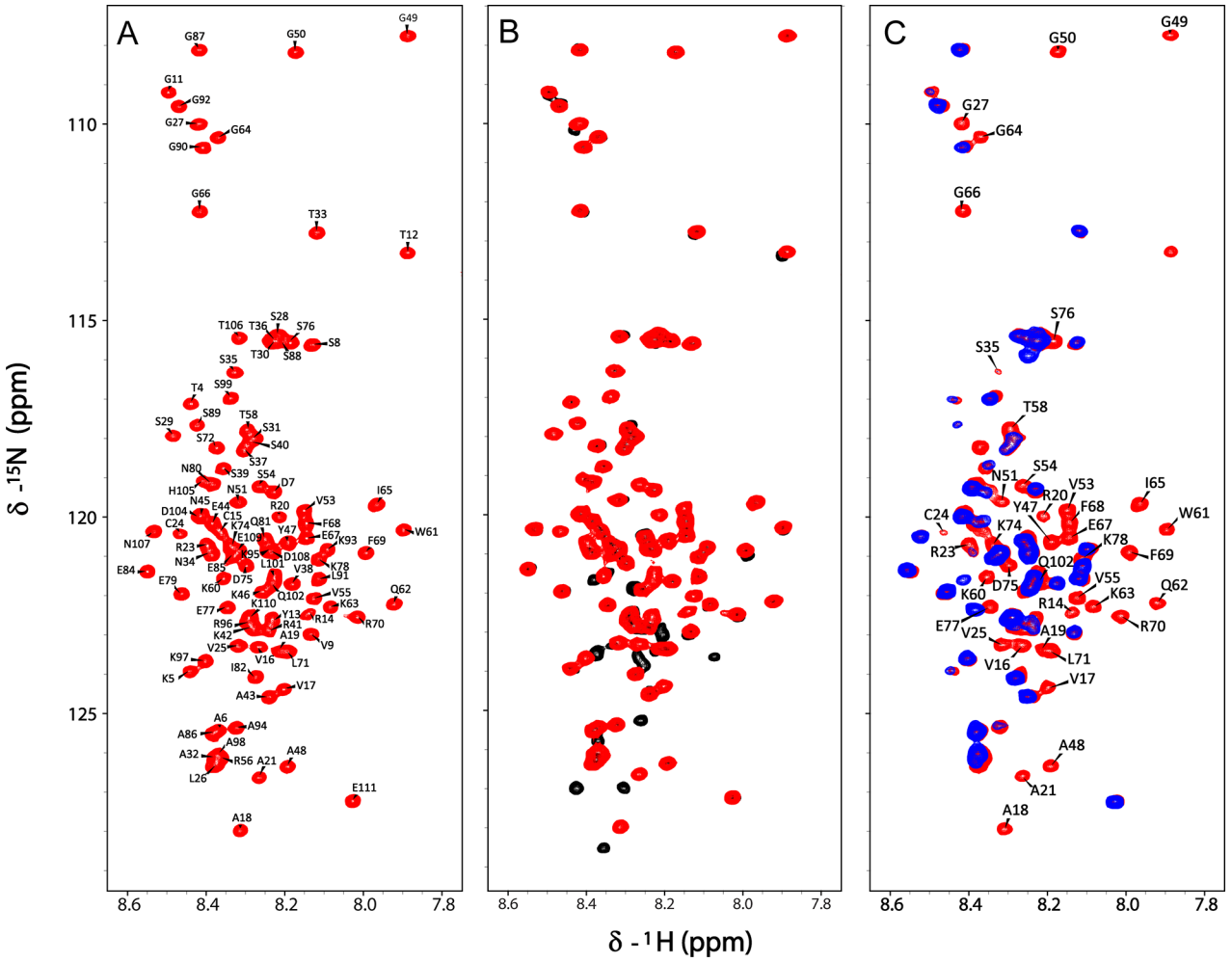

Figure 2. NMR fingerprint spectra of dmUbp15 with only p15 enriched in ^{15}N. (A) 2D ^{1}H,^{15}N HSQC NMR spectrum of dmUbp15 with assignment of the backbone amide signals (in PBS pH 6.2 at 25 °C and 800 MHz). (B) Overlay of dmUbp15 (red) and nonubiquitinated p15 (black). (C) Overlay of dmUbp15 spectra at pH 6.8 in the absence (red) and in the presence (blue) of PCNA at 1:4 molar ratio of PCNA protomer. The residues that suffer the highest intensity drop in the complex are labeled.

assigned amide signals (Figure 2A), where only the two N-terminal residues and the nine prolines (in the absence of an observable amide proton) are missing. All prolines have *trans* peptide bonds, as indicated by small [C^{α}−C^{β}] chemical shift differences.[21] A few minor signals with ca. 5% intensity of the major ones are visible in the ^{1}H,^{15}N HSQC spectrum (data not shown). At least one of these signals corresponds to a residue following a proline with a [C^{α}−C^{β}] chemical shift difference typical for a *cis*-configuration of the peptide bond. Therefore, we interpret the minor signals as arising from small populations of dmUbp15 proteins with peptidyl-prolyl *cis*-peptide bonds, as occurs with nonubiquitinated p15. The dispersion of backbone amide ^{1}H chemical shifts is similarly low for unmodified and for doubly monoubiquitinated p15 (Figure 2B), indicating that the latter remains disordered and flexible. The major changes occur at sites of ubiquitination and/or mutation (Figure S2). The distribution of p15 ^{15}N transverse relaxation rates, R_2, along the sequence (Figure S3) is likewise similar in both states except for the region between residues 11 and 27, which contains the ubiquitination sites (15 and 24). The approximately 2-fold increase in ^{15}N R_2 rates can, thus, be explained by a locally restricted mobility due to the attached ubiquitin moieties in dmUbp15. As in isolated p15, relatively large R_2 values are also found for residues 60 to 72, which could be explained by steric restrictions between bulky side chains and the backbone,[22] or by the presence of minor populations of nonrandom conformations.[14]

The chemical shift deviations for H^{α}, C', C^{α}, and C^{β} from random coil values (Figure 3), taken from intrinsically disordered proteins under native conditions,[23] do not indicate preferential local conformations in dmUbp15. Overall, our NMR data indicates the same level of intrinsic disorder and flexibility for p15 in the dmUbp15 fusion protein as in the previously analyzed isolated state.[14]

To further investigate the structural effects of ubiquitination in p15, we applied small-angle X-ray scattering (SAXS) as the best suited technique to probe the overall structure of disordered proteins.[24] Our synchrotron SEC-SAXS data revealed that dmUbp15 is a nonglobular particle in solution (Figure 4 A) with a radius of gyration (R_g) of 33.7 ± 0.4 Å and a maximum intermolecular distance (D_{max}) of 139.0 ± 10.0 Å (Figure 4B). dmUbp15 is slightly larger than nonubiquitinated p15CCSS, which has an R_g of 29.4 ± 0.5 Å and a D_{max} of 124.0 ± 5.0 Å (Figure 4A,B). The SAXS-derived structural parameters of p15CCSS are in the range of those previously measured for wild-type p15, R_g of 28.1 ± 0.3 Å and a D_{max} 120.0 ± 10.0 Å.[14] The Kratky representation of dmUbp15 SAXS data (Figure 4A) displays dual features. On the one

DOI: 10.1021/acschembio.9b00679
ACS Chem. Biol. 2019, 14, 2315−2326

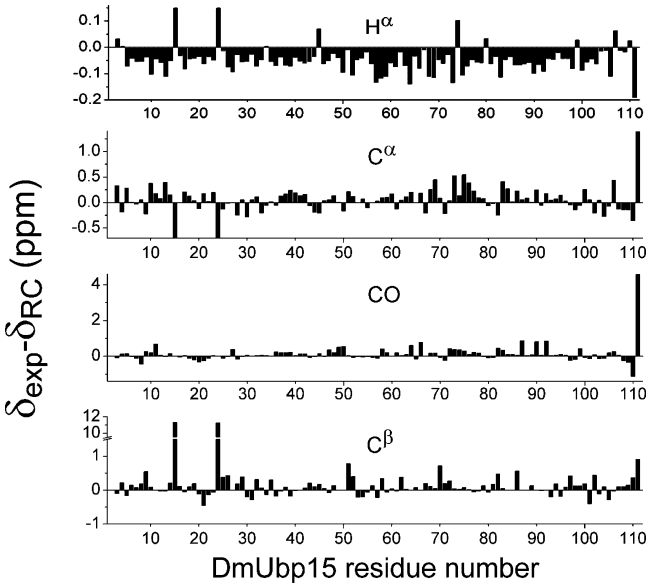

Figure 3. Experimental and random coil chemical shift[23] differences ($\delta_{exp} - \delta_{RC}$) versus dmUbp15 residue number, derived for the H^{α}, C^{α}, CO, and C^{β} nuclei in PBS buffer pH 6.2, 25 °C.

hand, it shows a broad peak, indicating an important level of compaction. On the other hand, this peak does not decrease completely, suggesting that p15 remains disordered upon dimonoubiquitination. Note that the Kratky representation of dmUbp15 is entirely different from that of p15CCSS, which displays a monotonous increase of $(sR_g)^2 \cdot I(s)$ at wide angles characteristic of fully disordered proteins (Figure 4A). The pairwise distance distribution, $P(r)$, of dmUbp15 (Figure 4B) also suggests this order−disorder duality. It is asymmetric with a smooth decrease toward a large D_{max}, as observed for highly flexible proteins like p15CCSS, but also displays two main peaks that encapsulate the intra- and interdomain pairwise distances of ubiquitin tags.[25] The SAXS data is, therefore, compatible with a protein containing folded domains tethered to a disordered region and is in clear contrast with those measured for ubiquitin, which is a globular protein.

To get more detailed structural information from the SAXS data, we applied the Ensemble Optimization Method (EOM).[26] The NMR analysis indicates that the presence of the two grafted ubiquitins does not perturb the conformational features of p15, which remains disordered in solution. Prompted by this observation, we have modeled the p15 protein as an IDP in both scenarios, with or without randomly oriented ubiquitin tags at residues 15 and 24. An atomistic ensemble model of the doubly monoubiquitinated p15 was built combining flexible-meccano (FM), molecular dynamics (MD) simulations, and in-house scripts (see methods for details). A second ensemble for p15CCSS was built by removing both ubiquitin moieties and the linkers from the dmUbp15 ensemble (Figure 4C). Using these structural pools, the EOM-derived ensembles provided an excellent fit to the experimental SAXS curves of p15CCSS and dmUbp15, with χ_i^2 values of 0.94 and 0.99, respectively (Figure 4D). The EOM-derived R_g distributions, compared with those obtained from the initial pools (before EOM), are displayed in Figures 4E and S4 for dmUbp15 and p15CCSS, respectively. These distributions sample a broad range of R_g values, indicating high flexibility of the protein regardless of the ubiquitination. Interestingly, both ensembles display an enrichment in extended conformations (large R_g values) when compared with the initial pools. This observation suggests that the transient secondary elements previously observed in wild-type p15 are also present in both cases[14] and substantiates the absence of major changes in the conformational sampling of p15 in the presence of the two covalently bound ubiquitin proteins, as also observed by NMR.

dmUbp15 Adopts Interubiquitin "*Closed*" and "*Open*" Conformations. SAXS is highly sensitive to the spatial distribution of globular domains within flexible proteins.[25] To exploit this feature, we analyzed the relative position of both ubiquitin moieties in the EOM-optimized ensemble of dmUbp15. By computing the distance between their centers of mass ($d_{Ub\text{-}Ub}$) for each conformer, we observed two families of structures that we classified as "*closed*" and "*open*". To better visualize these two families, we used a joint distribution of $d_{Ub\text{-}Ub}$ vs end-to-end distances (d_{ee}) of the structures from the initial pool (in gray) and the refined ensemble (in red) (Figure 4F). The pool, representing a random distribution of ubiquitin positions when grafted to dmUbp15, presents a single peak with a maximum at $d_{Ub\text{-}Ub}$ around 53 Å. Upon ensemble optimization against SAXS data, the single peak was resolved into two main clusters centered on $d_{Ub\text{-}Ub}$ values of 30.0 ± 4.0 Å and 52.4 ± 8.9 Å, hereafter named *closed* and *open* states, respectively. The inspection of the conformations belonging to the *closed* state indicates that both ubiquitin moieties are in contact, forming dimers in different three-dimensional arrangements. It is worth noting that both peaks in the optimized distribution appear isolated, and there is not a continuum of conformations between the closed and the open states. These observations indicate that, for doubly monoubiquitinated p15, the two ubiquitin moieties form a transient dimer. The presence of interubiquitin contacts does not perturb the overall size of the molecule, which remains highly disordered upon ubiquitination (Figures 4B−F). To further substantiate these observations, SAXS curves for the two states were computed by averaging the profiles of conformations belonging to each peak. Then, we performed a grid search by varying the relative population of the ensemble-based SAXS pattern representing the *closed* and *open* states. Although the minimum is relatively broad, the optimal level of agreement ($\chi^2 = 0.99$) with the SAXS curve of dmUbp15 was obtained at a 69/31 ratio for the *open/closed* models (Figure 4G and S5).

Ubiquitin has been reported to form highly dynamic symmetric dimers with very low affinity ($K_d \sim 5$ mM).[27] Using this dissociation constant and the relative population of the *open/closed* conformations derived from SAXS data, we estimated an effective ubiquitin concentration, C_{eff}, of 2.24 mM in the context of dmUbp15.[28] To further characterize the interaction between the two ubiquitin moieties within dmUbp15 and determine the dimerization surface, we recorded NMR spectra of singly monoubiquitinated p15 with only one ^{15}N-labeled ubiquitin molecule at position 15 or at position 24 (mUbp15_15 or mUbp15_24) and compared them with the spectrum of dmUbp15 (with two ^{15}N labeled ubiquitin chains). The differences in chemical shifts were very small (Figure S6) and do not match the interacting residues in ubiquitin dimers,[27] suggesting that the interaction detected by SAXS is too transient to be observed by NMR chemical shift differences.

DOI: 10.1021/acschembio.9b00679
ACS Chem. Biol. 2019, 14, 2315−2326

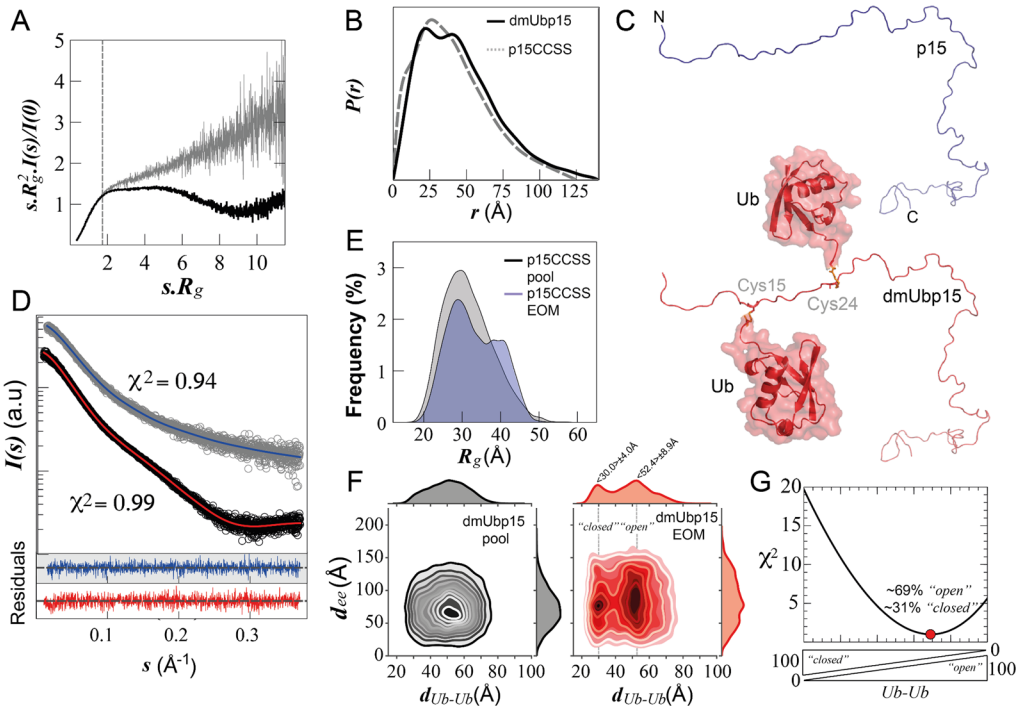

Figure 4. SAXS data analysis of dmUbp15 and p15CCSS in PBS pH 7.0 at 25 °C. (A) Dimensionless Kratky representation of the SEC-SAXS data measured for p15CCSS (gray) and dmUbp15 (black). The absence of a clear peak maximum at $sR_g = \sqrt{3}$ (dashed line) indicates that dmUbp15 remains conformationally heterogeneous upon ubiquitination. (B) Normalized pairwise distance distribution, $P(r)$, computed from experimental SAXS curves of p15CCSS (dashed gray line) and dmUbp15 (solid black line). As p15CCSS, dmUb1p15 has a large D_{max} and smooth ending to $P(D_{max}) = 0$. (C) Structural cartoon representation of p15CCSS (blue) and dmUbp15 (red). The linker connecting the ubiquitin tags to each cysteine residue is represented in yellow sticks. (D) Logarithmic-scale representation of scattering intensity, $I(s)$, as a function of the momentum transfer, s, measured for p15CCSS (empty gray circles) and dmUbp15 (empty black circles). Solid lines are averaged back-calculated curves derived from subensembles of p15CCSS (blue) and dmUbp15 (red) conformations derived from the EOM fit of the SAXS data. Residuals using absolute values are displayed at the bottom with the same color code, with a scale ranging from −4.0 to 4.0 (white and gray bands). (E) Comparison of the R_g distributions of the EOM-selected structures (blue) and the initial pool of 12 000 random-coil structures of p15CCSS (gray) built with flexible-meccano. The SAXS-based ensemble of p15CCSS is slightly more extended than the statistically random pool (~10% of enrichment). (F) Bivariate kernel density of the initial pool (gray-palette contours) and EOM-refined ensembles of dmUbp15 (red-palette contours) plotted in the d_{ee} and $d_{Ub\text{-}Ub}$ conformational space. SAXS data analysis reveals that dmUbp15 exists as a dynamic ensemble of conformations displaying a large population of states with short interubiquitin distances (*closed* state). (G) Evolution of χ^2 as a function of the relative population of *closed* and *open* states. A well-defined minimum is observed for an ensemble with ~31% of the *closed* state.

dmUbp15 Interacts with PCNA as Nonubiquitinated p15. The interaction of dmUbp15 with PCNA was studied by ITC and NMR. Calorimetry shows that one molecule of dmUbp15 binds to each protomer of PCNA with a K_d of 1.6 ± 0.1 μM at 25 °C (Figure S7 and Supplementary Table S1), which is similar to the isolated p15, with a K_d of 1.1 ± 0.1 μM [4]. The mutation C54S, within the PCNA binding region of p15, does not affect the affinity (K_d= 1.3 ± 0.1 μM, Figure S7 and Table S1). This result appears in contradiction with the previously reported promotion of PCNA binding by ubiquitination of p15 observed by nuclear colocalization.[6] Our quantitative calorimetry measurements demonstrate that ubiquitination does not affect the direct interaction between p15 and PCNA, and our NMR data shows that the PCNA binding mode of dmUbp15 is equivalent to that of p15 (Figure 2C). On the side of p15, this is indicated by the same general decrease in $^1H,^{15}N$ signal intensities and the same group of disappearing signals in the central region of the dmUbp15 chain (Figure S8).[4] On the side of PCNA, however, the $^1H,^{15}N$ TROSY spectrum only shows a few signals from its most flexible regions (Figure S9), most likely due to the slower tumbling rate of the complex (with an increased molar mass of ~180 kDa)

dmUbp15 Interacts with DNA with Reduced Affinity As Compared with Nonubiquitinated p15. p15 interacts with DNA in a sequence independent manner mainly through its N-terminal region,[4] which is rich in basic amino acids and contains both ubiquitination sites. Our working hypothesis was that double monoubiquitination of p15 might reduce its affinity for DNA via the neutralization of two positive charges (at the two lysine side chains) and via the increased steric hindrance exerted by the two attached ubiquitin moieties at the center of the DNA binding region at the p15 N-terminus. We examined this hypothesis by measuring the DNA affinity and 25 °C by NMR. This yielded a 5-fold reduced DNA affinity of dmUbp15 (K_d = 24 ± 3 μM; Figure 5) as compared with isolated p15 (K_d = 5 ± 1 μM). To further analyze whether the main inhibiting effect of p15 ubiquitination upon DNA binding is the entailed removal of two positive charges, rather than the increased steric hindrance, we also measured the DNA affinity of p15CCSS with double lysine-to-cysteine mutation and found a K_d = 91 ± 5 μM (Figure S10). This result clearly confirms the positive charge neutralization as the dominant effect of p15 ubiquitination upon DNA binding.

NMR analysis of ^{15}N labeled free ubiquitin (not conjugated with p15) shows that ubiquitin does not directly bind DNA,

DOI: 10.1021/acschembio.9b00679
ACS Chem. Biol. 2019, 14, 2315−2326

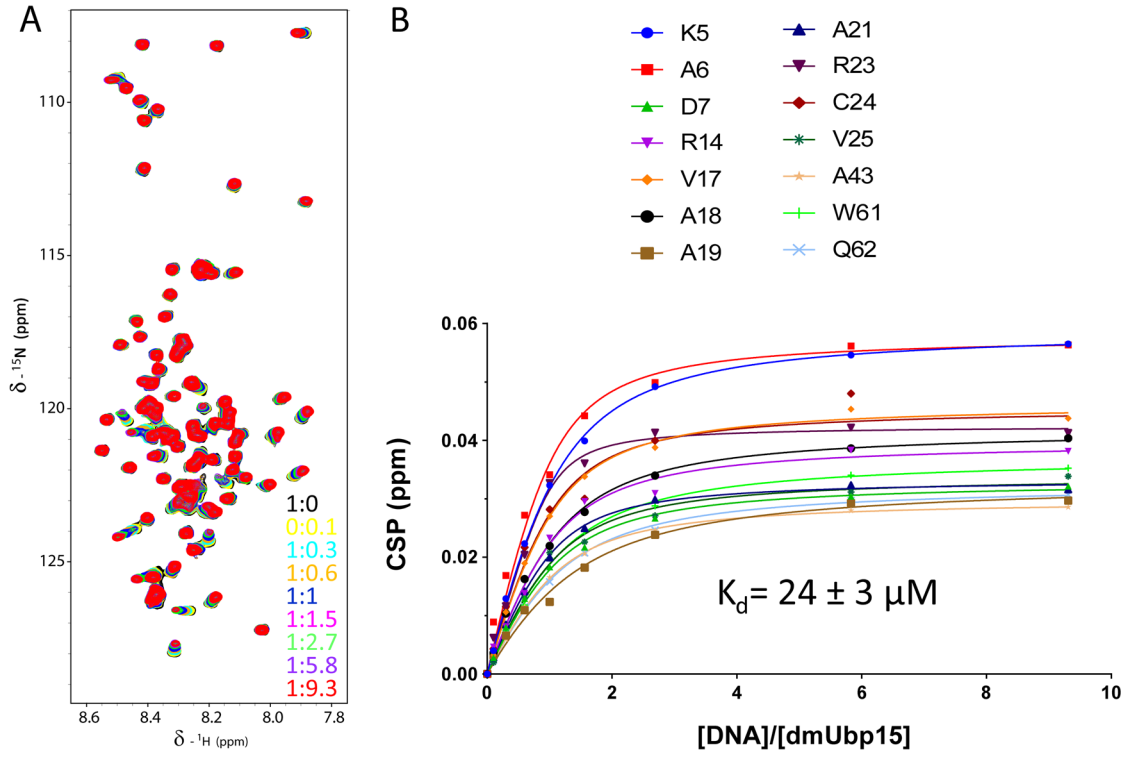

Figure 5. NMR analysis of dmUbp15 binding to a 24 bp DNA duplex (in PBS pH 6.2 at 25 °C). (A) Overlay of $^{1}H,^{15}N$ HSQC spectra at increasing DNA:dmUbp15 molar ratios with colors as indicated. (B) Chemical shift perturbation, CSP, versus DNA:dmUbp15 molar ratio for residues with CSP larger than the average plus one standard deviation. The indicated curves show fitting to a single-site binding model and yield *per residue* K_d values. The mean value of the dissociation constant and the standard error are indicated.

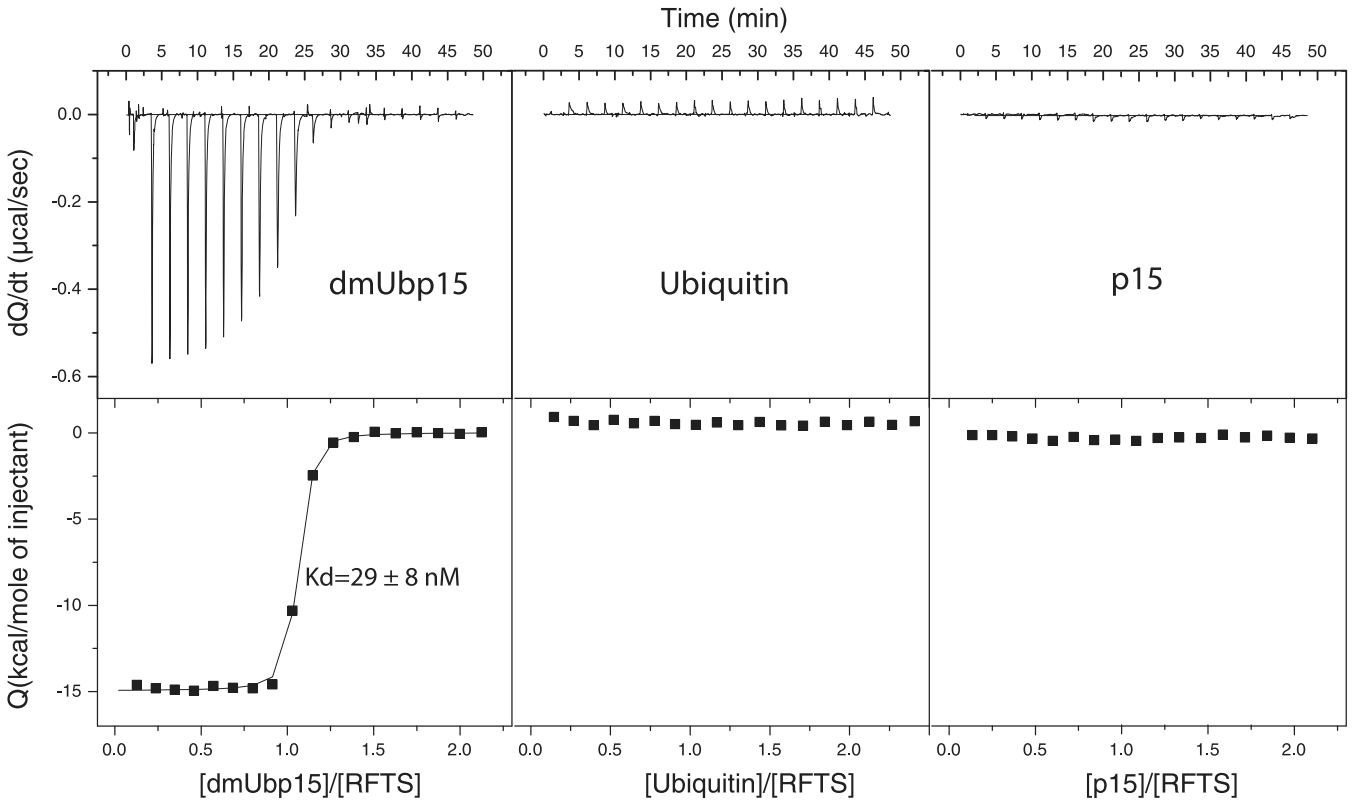

Figure 6. Calorimetric titration of dmUbp15, p15, and Ub with the RFTS domain of Dnmt1. The upper panel represents the heat effect associated with the peptide injection (differential power), and the lower panel represents the ligand concentration dependence of the heat released upon binding at 25 °C. Squares in the lower panels correspond to the experimental data and the continuous line to the best fit to a model of one set of identical binding sites.

DOI: 10.1021/acschembio.9b00679
ACS Chem. Biol. 2019, 14, 2315−2326

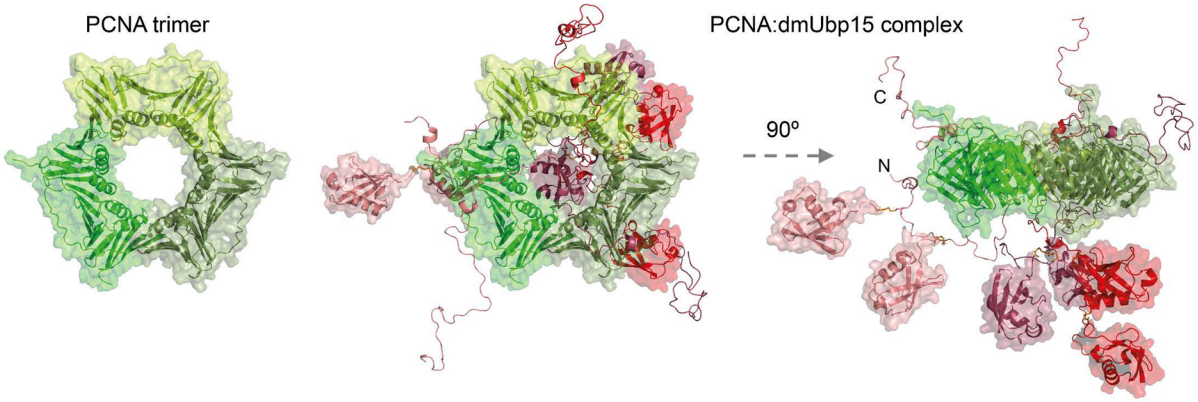

Figure 7. Model of the PCNA homotrimer (green gradation) with the maximum number of three bound dmUbp15 proteins. The largely unstructured p15 chains funnel through the PCNA ring and contact it via their PIP-box region.[4] dmUbp15 molecules, with two ubiquitin moieties at p15 residues 15 and 24, are colored in a red palette. The N- and C-termini of one of the p15 chains are indicated.

p15, or PCNA (Figure S11). However, by isotopically labeling only the ubiquitin moieties of dmUbp15, we measured small chemical shift perturbations in the presence of an excess of DNA (Figure S12 top). These perturbations occur mainly at the C-terminal end, the site of conjugation with p15, and are likely due to DNA binding to the positively charged arginine residues in this region, which enhances the overall DNA affinity of dmUbp15 as compared to p15CCSS. Even smaller perturbations were found in the chemical shifts of ubiquitin for dmUbp15 in the presence of PCNA (Figure S12 bottom).

The RFTS Domain of Dnmt1 Specifically Binds dmUbp15. The double monoubiquitination of p15, separated by eight disordered residues, makes it a favorable target for binding the reader module of DNA methyl transferase Dnmt1. This enzyme converts hemimethylated DNA (CpG methylated only in one of the strands) into its fully methylated form (in both strands), a crucial process in embryonic development.[29] Association of Dnmt1 with the replication machinery enhances methylation efficiency and occurs through a direct interaction of Dnmt1 with PCNA.[30,31] More recently it was shown that postreplicative DNA methylation is controlled by Dnmt1 recruitment to doubly monoubiquitinated histone H3.[15] The RFTS of Dnmt1 binds with nanomolar affinity (K_d = 18 ± 4 nM at 20 °C) the histone H3 N-terminal tail doubly monoubiquitinated at two lysine residues separated by three to eight residues.[15] We found that dmUbp15 is recognized by the RFTS domain of Dnmt1 with a similar affinity (K_d = 29.3 ± 4.5 nM at 25 °C; Figure 6). However, this binding is completely abolished when p15 is not ubiquitinated, in contrast to histone H3, which still binds with micromolar affinity.[15] To confirm that Dnmt1 specifically binds dmUbp15 we performed ITC experiments titrating monoubiquinated p15 at only one position (mUbp15_15 or mUbp15_24) with RFTS (Figure S12). Both monoubiquinated p15 molecules bind RFTS, but with a 20-fold lower affinity and an impaired stoichiometry (Table S2). These results indicate that double monoubiquitination of p15 is required for specific interaction with the RFTS domain of Dnmt1.

The structure of the complex is not known, but it is likely to be similar to that of the doubly monoubiquitinated histone H3 one, with the ubiquitin recognition loop of RFTS binding at the interface of both ubiquitin moieties. The preferential location of the two ubiquitin moieties close to each other in the conformational ensemble of dmUbp15, as observed by SAXS and the sequence similarity between the histone H3 and p15[4] support this hypothesis.

DISCUSSION

IDPs play diverse biological roles and structural disorder is important for the function of proteins that regulate processes often altered in cancer.[32] One of the functional advantages of IDPs presumably derives from their conformational adaptability, allowing for interactions with different biomolecular partners and for extensive regulation through post-translational modifications at many accessible sites.[33] Despite the lack of persistent structure, they can form fuzzy complexes[34] with low to very high affinity,[35] often driven by electrostatic forces. Conformational analysis of IDPs is challenging because their polypeptide backbone exhibits a high degree of flexibility with rapid interconversion of multiple conformers. NMR is then the method of choice for conformational analysis, together with SAXS, which has the capacity to report on the three-dimensional space sampled by disordered states and, thus, complements the local information provided by NMR.[26,36] The interest in IDPs has recently increased because of their involvement in the formation of membraneless organelles via protein phase separation.[37] Solutions of p15 or dmUbp15, however, do not show phase separation (at least up to 20 g/L at 25 °C), and our SEC-MALS data demonstrate that both are monomeric. Both proteins are intrinsically disordered, as confirmed by NMR. In the case of isolated p15, residual dipolar couplings showed the existence of low populations of nonrandom conformations in certain regions of the chain that could not be identified by local chemical shift deviation.[14] Possibly, dmUbp15 also shows some preferential local conformations, but these have too low populations for detection by chemical shift analysis (Figure 3). Ubiquitination causes only local perturbations in p15 chemical shifts and backbone dynamics, as sampled via ^{15}N NMR relaxation. Therefore, double ubiquitination does not change the intrinsically disordered nature of p15. SEC-SAXS data is also consistent with a disordered nature of the p15 chain in dmUbp15; however, these data also indicate that the ubiquitin-ubiquitin distance distribution is far from random, with an ensemble of conformations enriched in those with the ubiquitin moieties close to each other. This result is consistent with the observation of low affinity ubiquitin dimers in ubiquitin solutions[27] and with a high effective local

DOI: 10.1021/acschembio.9b00679
ACS Chem. Biol. 2019, 14, 2315−2326

concentration of ubiquitin in dmUbp15. The interaction of p15 with PCNA is unchanged by ubiquitination. Both p15 and dmUbp15 bind PCNA with the same low micromolar affinity through the central region of the p15 polypeptide chain. This result is in disagreement with the proposed promotion of PCNA binding by p15 ubiquitination.[6] Upon PCNA binding, p15 traverses the central channel of the PCNA ring, with its disordered N- and C-terminal regions emerging on opposite sides of the ring.[4,38] We assume that dmUbp15 adopts the same binding mode as it can still thread through the PCNA ring with its unmodified C-terminal end (Figure 7). Yet, dmUbp15 binds DNA with a 5-fold reduced affinity, and this effect could be interpreted in two ways: (i) removal of positive charge on the targeted lysines and its substitution by a globally neutral polypeptide chain (ubiquitin has a pI of 6.6) and (ii) steric impediment from attaching two ubiquitin globules (7 kDa each) at the N-terminal region of p15 that is mainly involved in DNA binding. The importance of the former charge effect is confirmed by an analysis of the p15CCSS mutant, whose affinity for DNA is reduced by a factor of 19. The steric effect seems to be much less important and is likely overridden by a favorable effect of the local positive charge at the C-terminal region of the ubiquitin molecule.

The reduced affinity of ubiquitinated p15 for DNA might have functional implications for the regulatory role of p15 on DNA replication and repair. Unperturbed DNA replication occurs with dmUbp15. In response to DNA damage, PCNA-bound dmUbp15 is degraded and replaced by nonubiquitinated p15, with higher DNA affinity, which may slow down the sliding of PCNA, thus facilitating the switch from replicative to translesion synthesis (TLS) polymerases.

At the same time, the double monoubiquitination of p15 separated by eight disordered residues makes it a target for binding the DNA methyl transferase Dnmt1, which also binds PCNA.[57] During unperturbed DNA replication p15 is doubly ubiquitinated and lies at the back face of the PCNA ring, because the N-terminal tail of p15 emerges from the back face. Therefore, dmUbp15 may act synergistically with PCNA to recruit and activate the Dnmt1 enzyme to the back of the replication fork (where the hemimethylated DNA localizes) to complete the methylation on the newly synthesized strand.

It has been shown that Dnmt1 is inhibited by its RFTS domain, which binds the catalytic domain to the exclusion of DNA.[39,40] Activation of Dnmt1 at specific times and locations is crucial for the maintenance of proper DNA methylation during cell proliferation, which ensures tissue- or cell-type-specific functions. Thus, constitutively active Dnmt1 leads to abnormal methylation patterns that affect this cell-type-specific functional differentiation. Previous studies proposed that the binding of H3 doubly monoubiquitinated at K18 and K23 to RFTS leads to Dnmt1 activation through dissociation of inserted RFTS from the catalytic domain.[15] Therefore, the two ubiquitin moieties act as a unique module recognized by the RFTS domain in an essential process to activate Dnmt1 at the proper time and location. Our results suggest that dmUbp15 binds RFTS and leads to the activation of Dnmt1 in the same way as doubly monoubiquitinated histone H3. Further studies should confirm if dmUbp15 activates Dnmt1 and whether this activation leads to a proper or abnormal function of Dnmt1. Future work will clarify the proposed role of dmUbp15 in the context of maintenance of DNA methylation.

METHODS

Protein Expression and Purification. The disulfide directed ubiquitination is a nonenzymatic method that requires the introduction of thiol groups both in ubiquitin and in the target protein. Thus, we designed a quadruple p15 mutant with the ubiquitination target lysines mutated to cysteine, whereas two native cysteines were mutated to serine. The amino acid sequence of human $p15^{PAF}$ used in this work corresponds to isoform 1, the canonical sequence of the full-length protein (Uniprot Q15004), with the following four mutations: K15C, K24C, C54S, and C99S (p15CCSS). We used a synthetic gene with a codon usage optimized for bacterial expression and cloned into a pET11d vector. The protein was expressed and purified as previously described for wild type p15.[14] Briefly, after BL21(DE3) bacterial growth at 37 °C in LB or M9 minimal medium with the appropriate isotopic enrichment (1 g/L 98% $^{15}NH_4Cl$ and 2 g/L 99% $^{13}C_6$-glucose) and after cell sonication, the protein was isolated from the supernatant by three chromatography steps at RT: anion exchange, reverse phase, and cation exchange. Then, a final reverse phase was done to be able to lyophilize the pure protein without buffer. After preparation for reverse-phase chromatography (by adding trifluoroacetic acid, TFA, to a final concentration of 0.1%), the solution was loaded on a Phenomenex Jupiter C_4 250 × 10 mm column with 10 μm particles and 300 Å pore diameter previously equilibrated with aqueous 0.1% TFA. The protein was eluted with a buffer gradient (to 90% aqueous acetonitrile, 0.1% TFA), eluting at approximately 40% acetonitrile. Fractions containing the protein (as seen by SDS-PAGE) were pooled and freeze-dried. In some instances, the protein was purified from the insoluble fraction by solubilization in 6 M urea and 10-fold dilution in water at pH 3.0, followed by reverse phase and cation exchange chromatography (plus a final reverse-phase step before lyophilization). Mass spectrometry measurements indicated that the initial methionine was partially processed by bacterial enzymes.

To prepare p15 mutants singly monoubiquitinated at positions 15 or 24, we reversed the mutation of one of the cysteines to lysine. Therefore, the new mutants could only be ubiquitinated at the remaining cysteine. The expression and purification strategy for these mutants was the same as for p15CCSS.

Human PCNA was produced and purified with or without isotope enrichment as described.[4]

The RFTS domain of human Dnmt1 (Uniprot P26358; residues 351−600) was produced from a synthetic gene that includes an N-terminal $MGSSH_6GSSG$ tag sequence followed by the human rhinovirus type 14 3C protease cleavage site. The protein was expressed in BL21(DE3) cells grown overnight at 20 °C in autoinducible ZYP5052 medium supplemented with 50 μM of $ZnCl_2$. After sonication, the protein was found in the pellet, solubilized with 8 M urea, and refolded by dropwise 50-fold dilution in 20 mM Tris pH 8, 300 mM NaCl, 1 mM DTT, 50 μM $ZnCl_2$, at 4 °C. The soluble protein was applied at RT to a His-Trap 5 mL Ni^{2+} column equilibrated in 20 mM Tris pH 8, 300 mM NaCl, 1 mM DTT, and was eluted with 250 mM imidazole. The fractions containing the protein were pooled and cleaved with the protease o/n at 4 °C while being dialyzed against 20 mM Tris pH 8.0, 1 mM DTT, to eliminate the imidazole. The dialyzed solution was applied to a His Trap column equilibrated in the same buffer and the flowthrough, containing the RFTS protein, was polished by gel filtration on a Superdex 200 26/60 column in PBS pH 7.0.

Ubiquitin fused to intein was prepared with natural isotope abundance or enriched in ^{15}N using the Ub-AvaDnaE-AAFN-H_6 clone[16] in BL21(DE3) cells, and was purified from the soluble fraction by Co^{2+} loaded HisTrap FF column in 20 mM Tris pH 8, 300 mM NaCl, 1 mM DTT (with or without 0.5 M imidazol).

The final protein concentration was determined by UV absorbance at 280 nm. After integrity checks by SDS-PAGE and MALDI-TOF, the proteins were stored at −80 °C.

Synthesis of Disulfide-Linked Doubly Monoubiquitinated p15. This synthesis was done as described before,[17] with some modifications. Ub-AvaDnaE-AAFN-H_6 protein[16] was dialyzed in 100

DOI: 10.1021/acschembio.9b00679
ACS Chem. Biol. 2019, 14, 2315−2326

mM sodium phosphate pH 7.8, 150 mM NaCl, 1 mM EDTA, 1 mM TCEP. The ubiquitin moiety was cleaved by adding 100 mM cysteamine and 50 mM TCEP, and incubating for 12 h at 25 °C. After adding 0.1% TFA, ubiquitin with C-terminal aminoethanethiol linker was purified by reverse-phase chromatography on a C_4 column with a gradient of 90% aqueous acetonitrile 0.1% TFA, eluting at approximately 50% acetonitrile. After lyophilization, a yield of 40 mg of Ub-SH per liter of culture was obtained. The Ub-SH protein was activated for ubiquitin linkage using 20.0 equiv of 2,2′-dithiobis(5-nitropyridine) (DTNP) in 2.0 mL of a 3:1 (v/v) acetic acid:water mixture. This solution was added to the Ub-SH powder, and the reaction proceeded for 72 h at 25 °C with agitation. Ubiquitin-S-nitro-2-pyridinesulfenyl disulfide adduct (Ub-DTNP) was purified by reverse-phase chromatography on a C_4 column, as described above.

Initially, 1.0 equiv of p15CCSS mutant (0.5 μmol) and 4.0 equiv of Ub-DTNP (2 μmol) were dissolved in 1 M HEPES (10 mL) pH 6.8 and shaken at 25 °C for 1 h. Ubiquitin-conjugated p15 was purified by C_4 reverse-phase chromatography to yield ca. 0.15 μmol (30%) of dmUbp15. The sample identity and purity were confirmed by MALDI-TOF and SDS-PAGE (Figure S1). An equivalent procedure was used to obtain the singly monoubiquitinated mUbp15_15 and mUbp15_24 molecules. Notably, both ubiquitin and p15 mutants used in this coupling reaction could have distinct isotope enrichment for subsequent NMR studies.

Size-Exclusion Chromatography-Multi Angle Light Scattering (SEC-MALS). This experiment was performed at 25 °C using a Superdex 200 10/300 GL column (GE HealthCare) connected to a DAWN-HELEOS light scattering detector and an Optilab rEX differential refractive index detector (Wyatt Technology). The column was equilibrated with 0.1 μm filtered PBS (10 mM phosphate, 140 mM chloride, 153 mM sodium, 4.5 mM potassium) at pH 7.0, and the SEC-MALS system was calibrated with a sample of bovine serum albumin (BSA) at 1 g/L in the same buffer. Next, 0.1 mL of dmUbp15 protein at 1 g/L was injected at 0.5 mL/min. The data was acquired and analyzed by ASTRA (Wyatt). From repeated measurements of BSA samples at 1 g/L under identical or similar conditions we estimate an experimental error of ca. 5% in the molar mass.

CD Spectroscopy. Spectra of 3 μM dmUbp15 or p15CCSS samples in PBS pH 7.0 were recorded on a Jasco-815 spectropolarimeter at 25 °C in a quartz cuvette (path length 2 mm).

NMR Spectroscopy. All NMR experiments were recorded at 35 °C (for observation of PCNA) and 25 °C (for observation of dmUbp15 or free ubiquitin) on a Bruker Avance III spectrometer operating at 18.8 T (800 MHz ^{1}H Larmor frequency) and equipped with a TCI cryo-probe and z gradients. Spectra were processed with TopSpin (Bruker) and analyzed using Sparky.[41] ^{1}H chemical shifts were referenced directly, ^{13}C and ^{15}N chemical shifts indirectly,[42] to added 2,2-dimethyl-2-silapentane-5-sulfonate (DSS, methyl ^{1}H signal at 0.00 ppm). Spectra for p15 backbone assignment were recorded using a 150 μM dmUbp15 [U−^{13}C,^{15}N] sample (with unlabeled ubiquitin) in PBS, pH 6.2, 5% (v/v) ^2H_2O, 0.01% NaN_3. The p15 resonance assignment was derived from a set of 3D HNCO, HN(CA)CO, HNCA, HN(CO)CA, HNCACB, HN(CO)CACB, HN(CA)HA, and HN(COCA)HA experiments, all implemented as BEST−TROSY version.[43] Automatic assignment of backbone and $^{13}C^{\beta}$ resonances was obtained with MARS[44] and completed manually. The assignment for p15CCSS mutant was obtained in a similar way except that the sample was 50 μM and that no $^{13}C^{\beta}$ or $^1H^{\alpha}$ resonances were assigned. The NMR resonance assignment for p15CCSS and dmUbp15 have been deposited in the BioMagResBank with the entries 27 698 and 27 696, respectively. Secondary chemical shift values were calculated from the difference between measured $^1H^{\alpha}$, $^{13}C'$, $^{13}C^{\alpha}$, $^{13}C^{\beta}$ chemical shifts and their amino acid specific random-coil values.[23] Backbone amide ^{15}N transverse (T_2) relaxation times were measured from a series of 2D ^{1}H−^{15}N HSQC spectra modulated by ^{15}N CPMG periods[45] of different duration (16.02, 48.05, 96.09, 160.16, 256.26, and 400.4 ms). These spectra were acquired in an interleaved mode, and signal intensities were fitted to a single exponential decay. Signal overlap prevented reliable intensity measurement for some residues that were not included in the further analysis.

For titrations of dmUbp15 with dsDNA, we used a 65 μM protein sample in PBS pH 6.2 and a stock solution of concentrated dsDNA (1.72 mM) in the same buffer.[4] The dsDNA was formed by a 5′-TCAACATGATGTTCATAATCCCAA-3′oligonucleotide and its reverse complementary sequence. This was the same dsDNA that was used to measure the p15 interaction with DNA.[4] The dissociation constants (K_d) were derived from those residues that at the last point of the titration showed a weighted[46] amide ^{1}H and ^{15}N chemical shift perturbation (CSP) larger than the average plus one standard deviation. The CSP values along the titration were fitted to a 1:1 binding model for each residue, and reported K_d values are the mean ± the standard error of the mean.

Molecular Modeling and Small-Angle X-ray Scattering. A random coil ensemble of p15CCSS containing ca. 15 000 conformations was calculated by flexible-meccano (FM)[47,48] followed by side-chain modeling with SCCOMP[49] and energy-refinement in explicit solvent using GROMACS 5.1.1.[50] In parallel, we created a structural library for the aminoethanethiol linker (NH_2-CH_2-CH_2-SH) by running a molecular dynamics (MD) simulation of a neutral Ac-GlyGlyCysGlyGly-NH_2 peptide (PET5, with acetylated and amidated N and C termini) in water at 25 °C, where the linker was attached to the central cysteine residue and prepended by Ac-Gly to mimic a minimal protein context (i.e., Ac-Gly-CO-NH-CH_2-CH_2-**S**-S-CH_2-PET5). We used the force field AMBER99sb-ILDN[51] with no ions added and TIP3P[52] as the water model. The system was equilibrated for 0.2 ns in the NVT ensemble and then for another 0.2 ns in the NPT ensemble with a 2 fs time-step. The production MD run spanned 14 ns, and from the last 10 ns, a frame was extracted every 10 ps to create a library of 1 000 different linker positions. From this library, the two engineered cysteine residues of each p15CCSS structure were labeled in silico with one randomly selected and sterically allowed linker conformation, followed by grafting an ubiquitin-moiety (PDB: 1UBQ), with flexible C-terminal residues 74−76, onto the amino group of the attached linker (i.e., Ub-Gly76-CO-NH-CH_2-CH_2−S-S-CH_2-Cys15/24-p15), resulting in 12 000 doubly ubiquitinated p15 (dmUbp15) conformers with no steric clashes. To obtain the equivalent pool of p15CCSS conformers, we removed the linkers and the Ub-tags, so that each dmUbp15 conformer had its untagged version. We also created an ensemble model of PCNA-dmUbp15 complex with three dmUbp15 molecules bound to PCNA trimer via the PIP-Box region, as observed in the crystal structure of the PCNA-p15 complex.[4]

Synchrotron SEC-SAXS data were collected at 25 °C on the B21 beamline at the Diamond Light Source (Didcot, U.K.) using an in-line Agilent HPLC system. Samples of 45 μL with 5.05 and 13.05 g/L of p15CCSS and dmUbp15, respectively, were injected into a 4.6 mL Shodex KW402.5-4F size exclusion column at a flow rate of 0.16 mL min^{-1}. The SEC mobile phase consisted of PBS pH 7.0 (plus 1 mM DTT in the case of p15CCSS). Two-second frames were acquired using a Pilatus 2 M pixel detector (DECTRIS) at a sample−detector distance of 4 m and a wavelength of λ = 1.0 Å, covering a moment of transfer range of $0.0032 < s < 0.37$ Å^{-1}. Scattering intensities from p15CCSS and dmUbp15 SEC-peak regions were integrated and buffer subtracted to produce the SAXS-profile from each sample using the ScÅtter software.[53] From the profiles the pairwise distance distribution functions, $P(r)$, were obtained by indirect Fourier Transform with GNOM[54] using a momentum transfer range of $0.010 < s < 0.37$ Å^{-1}. The R_g values were estimated by applying the Guinier approximation in the range $s < 0.8/R_g$ for p15CCSS and $s < 1.3/R_g$ for dmUbp15. We used CRYSOL[55] to compute the theoretical SAXS profiles from conformational ensembles of untagged p15CCSS and doubly ubiquitinated dmUbp15. All theoretical curves were obtained with 101 points and a maximum scattering vector of 0.37 Å^{-1} using 25 harmonics. Assuming that p15 remains disordered upon ubiquitination, we employed the ensemble optimization method (EOM)[26] to select from the p15CCSS and dmUbp15 structure pools, a set of 50 conformers whose theoretical SAXS profiles fit the SEC-SAXS profiles obtained for p15CCSS and dmUbp15. EOM was

DOI: 10.1021/acschembio.9b00679
ACS Chem. Biol. 2019, 14, 2315−2326

performed by minimizing the χ^2 between experimental (I^j_{exp}) and average theoretical (I^j_{theo}) SAXS intensities:

$$\chi_j^2 = \frac{1}{K-1}\sum_{i=1}^{K}\left[\frac{I^j_{exp}(s_i) - \mu I^j_{theo}(s_i)}{\sigma(s_i)}\right]^2$$

where K is the number of data points of each SEC-SAXS profile (I^j_{exp}), $\sigma(s)$ the standard deviations of the scattering intensity, and μ a scaling factor. I^j_{theo} was obtained by averaging the scattering of 50 explicit models per species (i.e., j = p15CCSS or dmUbp15):

$$I^j_{theo}(s) = \frac{1}{N}\sum_{1}^{N=50} j(s)$$

By running EOM multiple times (i.e., 220 runs) we were able to compare the R_g distribution and joint distribution of distances between the centers of mass of the two ubiquitin moieties ($d_{Ub\text{-}Ub}$) vs end-to-end distances (d_{ee}) of the selected ensemble and the initial pool.

Isothermal Titration Calorimetry. For dmUbp15 binding to PCNA, we employed a Microcal iTC200 calorimeter with 25 μM PCNA in the cell at 25 °C. The PCNA protein solution (dialyzed against PBS, pH 7.0) was titrated with a 0.4 mM stock solution of dmUbp15 prepared by dissolving the lyophilized material in the dialysis buffer and adjusting the pH to 7.0 with NaOH. For binding to p15CCSS and p15C54S, PCNA was dialyzed against PBS pH 7.0, 2 mM TCEP. PCNA 20 μM solutions in the cell were titrated with 400 μM of the corresponding p15 variant. The binding isotherms were analyzed by nonlinear least-squares fitting of the experimental data to a model assuming a single set of equivalent sites,[56] using Microcal Origin (OriginLab).

For experiments with the RFTS domain of Dnmt1, we used a Microcal PEAQ-ITC (Malvern) calorimetry system. dmUbp15, mUbp15_15, mUbp15_24, p15, or ubiquitin were placed in the cell and RFTS in the syringe, in PBS, pH 7.0. The binding isotherms were analyzed by nonlinear least-squares fitting of the experimental data to a model assuming a single set of equivalent sites, using the Malvern software and plotted with Origin. All the experiments were performed at 25 °C.

■ ASSOCIATED CONTENT

Supporting Information

The Supporting Information is available free of charge on the ACS Publications website at DOI: 10.1021/acschembio.9b00679.

SDS-PAGE analysis, chemical shifts deviations, transverse ^{15}N relaxation R_2 values, comparative SAXS data of p15CCSS and dmUbp15 to the monomeric globular ubiquitin, comparative experimental and calculated SAXS data before and after conformational ensemble optimization, overlay of ^1H-^{15}N HSQC spectra, calorimetric titrations of PCNA with dmUbp15 or p15 mutant C54S, NMR signal intensities measured in the 2D ^1H,^{15}N HSQC spectra of dmUbp15 in the absence or presence of PCNA, overlay of ^1H,^{15}N TROSY spectra of perdeuterated PCNA [U-^2H,^{15}N] in the absence or presence of unlabeled dmUbp15, NMR analysis of p15CCSS, overlay of ^1H-^{15}N HSQC spectra, calorimetric titrations, thermodynamic parameters of the binding of p15 molecules to PCNA, thermodynamic parameters of the binding of RFTS to different p15 molecules, and supporting references (PDF)

■ AUTHOR INFORMATION

Corresponding Author

*E-mail: fblanco@cicbiogune.es.

ORCID

Javier Murciano-Calles: 0000-0002-8667-1651

Francisco J. Blanco: 0000-0003-2545-4319

Notes

The authors declare no competing financial interest.

■ ACKNOWLEDGMENTS

Spanish Ministerio de Economía y Competitividad and the Fondo Europeo de Desarrollo Regional (MINECO/FEDER) [CTQ2017-83810-R to F.J.B.]; Labex EpiGenMed, an "Investissements d"avenir' program [ANR-10-LABX-12-01 to PB]. MOSTMicro [LISBOA-01-0145-FEDER-007660 to T.N.C. and H.M.]. A.G.M. acknowledges Spanish MINECO for predoctoral contract BE-2015-075847, and the CIC bioGUNE acknowledges MINECO for the Severo Ochoa accreditation Sev-2016-0644. The CBS-Montpellier is a member of France-BioImaging (FBI) and the French Infrastructure for Integrated Structural Biology (FRISBI), two national infrastructures supported by the French National Research Agency (ANR-10-INSB-04-01 and ANR-10-INSB-05, respectively). We acknowledge the use of B21 beamline at the Diamond Light Source (DSL, U.K.) facility. We thank T. W. Muir and M. R. Pratt for the ubiquitin-intein clone and guidance on the disulfide formation reaction.

■ REFERENCES

(1) Bah, A., and Forman-Kay, J. D. (2016) Modulation of Intrinsically Disordered Protein Function by Post-translational Modifications. *J. Biol. Chem. 291*, 6696−6705.

(2) Yu, P., Huang, B., Shen, M., Lau, C., Chan, E., Michel, J., Xiong, Y., Payan, D. G., and Luo, Y. (2001) p15(PAF), a novel PCNA associated factor with increased expression in tumor tissues. *Oncogene 20*, 484−489.

(3) Moldovan, G. L., Pfander, B., and Jentsch, S. (2007) PCNA, the maestro of the replication fork. *Cell 129*, 665−679.

(4) De Biasio, A., de Opakua, A. I., Mortuza, G. B., Molina, R., Cordeiro, T. N., Castillo, F., Villate, M., Merino, N., Delgado, S., Gil-Carton, D., Luque, I., Diercks, T., Bernado, P., Montoya, G., and Blanco, F. J. (2015) Structure of p15(PAF)-PCNA complex and implications for clamp sliding during DNA replication and repair. *Nat. Commun. 6*, 6439.

(5) Povlsen, L. K., Beli, P., Wagner, S. A., Poulsen, S. L., Sylvestersen, K. B., Poulsen, J. W., Nielsen, M. L., Bekker-Jensen, S., Mailand, N., and Choudhary, C. (2012) Systems-wide analysis of ubiquitylation dynamics reveals a key role for PAF15 ubiquitylation in DNA-damage bypass. *Nat. Cell Biol. 14*, 1089−1098.

(6) Karg, E., Smets, M., Ryan, J., Forne, I., Qin, W., Mulholland, C. B., Kalideris, G., Imhof, A., Bultmann, S., and Leonhardt, H. (2017) Ubiquitome Analysis Reveals PCNA-Associated Factor 15 (PAF15) as a Specific Ubiquitination Target of UHRF1 in Embryonic Stem Cells. *J. Mol. Biol. 429*, 3814−3824.

(7) Nishiyama, A., Yamaguchi, L., Sharif, J., Johmura, Y., Kawamura, T., Nakanishi, K., Shimamura, S., Arita, K., Kodama, T., Ishikawa, F., Koseki, H., and Nakanishi, M. (2013) Uhrf1-dependent H3K23 ubiquitylation couples maintenance DNA methylation and replication. *Nature 502*, 249−253.

(8) Qin, W., Wolf, P., Liu, N., Link, S., Smets, M., La Mastra, F., Forne, I., Pichler, G., Horl, D., Fellinger, K., Spada, F., Bonapace, I. M., Imhof, A., Harz, H., and Leonhardt, H. (2015) DNA methylation requires a DNMT1 ubiquitin interacting motif (UIM) and histone ubiquitination. *Cell Res. 25*, 911−929.

(9) Hosokawa, M., Takehara, A., Matsuda, K., Eguchi, H., Ohigashi, H., Ishikawa, O., Shinomura, Y., Imai, K., Nakamura, Y., and Nakagawa, H. (2007) Oncogenic role of KIAA0101 interacting with proliferating cell nuclear antigen in pancreatic cancer. *Cancer Res. 67*, 2568−2576.

DOI: 10.1021/acschembio.9b00679
ACS Chem. Biol. 2019, 14, 2315−2326

(10) Kato, T., Daigo, Y., Aragaki, M., Ishikawa, K., Sato, M., and Kaji, M. (2012) Overexpression of KIAA0101 predicts poor prognosis in primary lung cancer patients. *Lung Cancer 75*, 110−118.
(11) Liu, L., Chen, X., Xie, S., Zhang, C., Qiu, Z., and Zhu, F. (2012) Variant 1 of KIAA0101, overexpressed in hepatocellular carcinoma, prevents doxorubicin-induced apoptosis by inhibiting p53 activation. *Hepatology 56*, 1760−1769.
(12) Wang, X., Jung, Y. S., Jun, S., Lee, S., Wang, W., Schneider, A., Sun Oh, Y., Lin, S. H., Park, B. J., Chen, J., Keyomarsi, K., and Park, J. I. (2016) PAF-Wnt signaling-induced cell plasticity is required for maintenance of breast cancer cell stemness. *Nat. Commun. 7*, 10633.
(13) Ong, D. S. T., Hu, B., Ho, Y. W., Sauve, C. G., Bristow, C. A., Wang, Q., Multani, A. S., Chen, P., Nezi, L., Jiang, S., Gorman, C. E., Monasterio, M. M., Koul, D., Marchesini, M., Colla, S., Jin, E. J., Sulman, E. P., Spring, D. J., Yung, W. A., Verhaak, R. G. W., Chin, L., Wang, Y. A., and DePinho, R. A. (2017) PAF promotes stemness and radioresistance of glioma stem cells. *Proc. Natl. Acad. Sci. U. S. A. 114*, E9086−E9095.
(14) De Biasio, A., Ibañez de Opakua, A., Cordeiro, T. N., Villate, M., Merino, N., Sibille, N., Lelli, M., Diercks, T., Bernadó, P., and Blanco, F. J. (2014) p15(PAF) Is an Intrinsically Disordered Protein with Nonrandom Structural Preferences at Sites of Interaction with Other Proteins. *Biophys. J. 106*, 865−874.
(15) Ishiyama, S., Nishiyama, A., Saeki, Y., Moritsugu, K., Morimoto, D., Yamaguchi, L., Arai, N., Matsumura, R., Kawakami, T., Mishima, Y., Hojo, H., Shimamura, S., Ishikawa, F., Tajima, S., Tanaka, K., Ariyoshi, M., Shirakawa, M., Ikeguchi, M., Kidera, A., Suetake, I., Arita, K., and Nakanishi, M. (2017) Structure of the Dnmt1 Reader Module Complexed with a Unique Two-Mono-Ubiquitin Mark on Histone H3 Reveals the Basis for DNA Methylation Maintenance. *Mol. Cell 68*, 350−360.
(16) Shah, N. H., Dann, G. P., Vila-Perello, M., Liu, Z., and Muir, T. W. (2012) Ultrafast protein splicing is common among cyanobacterial split inteins: implications for protein engineering. *J. Am. Chem. Soc. 134*, 11338−11341.
(17) Abeywardana, T., Lin, Y. H., Rott, R., Engelender, S., and Pratt, M. R. (2013) Site-specific differences in proteasome-dependent degradation of monoubiquitinated alpha-synuclein. *Chem. Biol. 20*, 1207−1213.
(18) Faggiano, S., and Pastore, A. (2014) The challenge of producing ubiquitinated proteins for structural studies. *Cells 3*, 639−656.
(19) Morimoto, D., Walinda, E., Fukada, H., Sou, Y. S., Kageyama, S., Hoshino, M., Fujii, T., Tsuchiya, H., Saeki, Y., Arita, K., Ariyoshi, M., Tochio, H., Iwai, K., Namba, K., Komatsu, M., Tanaka, K., and Shirakawa, M. (2015) The unexpected role of polyubiquitin chains in the formation of fibrillar aggregates. *Nat. Commun. 6*, 6116.
(20) De March, M., Barrera-Vilarmau, S., Crespan, E., Mentegari, E., Merino, N., Gonzalez-Magana, A., Romano-Moreno, M., Maga, G., Crehuet, R., Onesti, S., Blanco, F. J., and De Biasio, A. (2018) p15PAF binding to PCNA modulates the DNA sliding surface. *Nucleic Acids Res. 46*, 9816−9828.
(21) Schubert, M., Labudde, D., Oschkinat, H., and Schmieder, P. (2002) A software tool for the prediction of Xaa-Pro peptide bond conformations in proteins based on 13C chemical shift statistics. *J. Biomol. NMR 24*, 149−154.
(22) Cho, M. K., Kim, H. Y., Bernado, P., Fernandez, C. O., Blackledge, M., and Zweckstetter, M. (2007) Amino acid bulkiness defines the local conformations and dynamics of natively unfolded alpha-synuclein and tau. *J. Am. Chem. Soc. 129*, 3032−3033.
(23) Tamiola, K., Acar, B., and Mulder, F. A. (2010) Sequence-specific random coil chemical shifts of intrinsically disordered proteins. *J. Am. Chem. Soc. 132*, 18000−18003.
(24) Cordeiro, T. N., Herranz-Trillo, F., Urbanek, A., Estana, A., Cortes, J., Sibille, N., and Bernado, P. (2017) Small-angle scattering studies of intrinsically disordered proteins and their complexes. *Curr. Opin. Struct. Biol. 42*, 15−23.
(25) Bernado, P. (2010) Effect of interdomain dynamics on the structure determination of modular proteins by small-angle scattering. *Eur. Biophys. J. 39*, 769−780.
(26) Bernado, P., Mylonas, E., Petoukhov, M. V., Blackledge, M., and Svergun, D. I. (2007) Structural characterization of flexible proteins using small-angle X-ray scattering. *J. Am. Chem. Soc. 129*, 5656−5664.
(27) Liu, Z., Zhang, W. P., Xing, Q., Ren, X., Liu, M., and Tang, C. (2012) Noncovalent dimerization of ubiquitin. *Angew. Chem., Int. Ed. 51*, 469−472.
(28) Zhou, H. X. (2003) Quantitative account of the enhanced affinity of two linked scFvs specific for different epitopes on the same antigen. *J. Mol. Biol. 329*, 1−8.
(29) Smith, Z. D., and Meissner, A. (2013) DNA methylation: roles in mammalian development. *Nat. Rev. Genet. 14*, 204−220.
(30) Chuang, L. S., Ian, H. I., Koh, T. W., Ng, H. H., Xu, G., and Li, B. F. (1997) Human DNA-(cytosine-5) methyltransferase-PCNA complex as a target for p21WAF1. *Science 277*, 1996−2000.
(31) Schermelleh, L., Haemmer, A., Spada, F., Rosing, N., Meilinger, D., Rothbauer, U., Cardoso, M. C., and Leonhardt, H. (2007) Dynamics of Dnmt1 interaction with the replication machinery and its role in postreplicative maintenance of DNA methylation. *Nucleic Acids Res. 35*, 4301−4312.
(32) Dyson, H. J., and Wright, P. E. (2005) Intrinsically unstructured proteins and their functions. *Nat. Rev. Mol. Cell Biol. 6*, 197−208.
(33) Tompa, P., and Fuxreiter, M. (2008) Fuzzy complexes: polymorphism and structural disorder in protein-protein interactions. *Trends Biochem. Sci. 33*, 2−8.
(34) Sharma, R., Raduly, Z., Miskei, M., and Fuxreiter, M. (2015) Fuzzy complexes: Specific binding without complete folding. *FEBS Lett. 589*, 2533−2542.
(35) Wang, Y., Bugge, K., Kragelund, B. B., and Lindorff-Larsen, K. (2018) Role of protein dynamics in transmembrane receptor signalling. *Curr. Opin. Struct. Biol. 48*, 74−82.
(36) Ibanez de Opakua, A., Merino, N., Villate, M., Cordeiro, T. N., Ormaza, G., Sanchez-Carbayo, M., Diercks, T., Bernado, P., and Blanco, F. J. (2017) The metastasis suppressor KISS1 is an intrinsically disordered protein slightly more extended than a random coil. *PLoS One 12*, No. e0172507.
(37) Boeynaems, S., Alberti, S., Fawzi, N. L., Mittag, T., Polymenidou, M., Rousseau, F., Schymkowitz, J., Shorter, J., Wolozin, B., Van Den Bosch, L., Tompa, P., and Fuxreiter, M. (2018) Protein Phase Separation: A New Phase in Cell Biology. *Trends Cell Biol. 28*, 420−435.
(38) Cordeiro, T. N., Chen, P. C., De Biasio, A., Sibille, N., Blanco, F. J., Hub, J. S., Crehuet, R., and Bernado, P. (2017) Disentangling polydispersity in the PCNA-p15PAF complex, a disordered, transient and multivalent macromolecular assembly. *Nucleic Acids Res. 45*, 1501−1515.
(39) Syeda, F., Fagan, R. L., Wean, M., Avvakumov, G. V., Walker, J. R., Xue, S., Dhe-Paganon, S., and Brenner, C. (2011) The replication focus targeting sequence (RFTS) domain is a DNA-competitive inhibitor of Dnmt1. *J. Biol. Chem. 286*, 15344−15351.
(40) Takeshita, K., Suetake, I., Yamashita, E., Suga, M., Narita, H., Nakagawa, A., and Tajima, S. (2011) Structural insight into maintenance methylation by mouse DNA methyltransferase 1 (Dnmt1). *Proc. Natl. Acad. Sci. U. S. A. 108*, 9055−9059.
(41) Goddar, T. D., and Kneller, D. G. *Sparky—NMR Assignment and Integration Software, 3.0*; University of California, San Francisco, 2008.
(42) Wishart, D. S., Bigam, C. G., Yao, J., Abildgaard, F., Dyson, H. J., Oldfield, E., Markley, J. L., and Sykes, B. D. (1995) ^{1}H, ^{13}C and ^{15}N chemical shift referencing in biomolecular NMR. *J. Biomol. NMR 6*, 135−140.
(43) Solyom, Z., Schwarten, M., Geist, L., Konrat, R., Willbold, D., and Brutscher, B. (2013) BEST-TROSY experiments for time-efficient sequential resonance assignment of large disordered proteins. *J. Biomol. NMR 55*, 311−321.

DOI: 10.1021/acschembio.9b00679
ACS Chem. Biol. 2019, 14, 2315−2326

(44) Jung, Y. S., Sharma, M., and Zweckstetter, M. (2004) Simultaneous assignment and structure determination of protein backbones by using NMR dipolar couplings. *Angew. Chem., Int. Ed. 43*, 3479−3481.
(45) Farrow, N. A., Muhandiram, R., Singer, A. U., Pascal, S. M., Kay, C. M., Gish, G., Shoelson, S. E., Pawson, T., Forman-Kay, J. D., and Kay, L. E. (1994) Backbone dynamics of a free and phosphopeptide-complexed Src homology 2 domain studied by 15N NMR relaxation. *Biochemistry 33*, 5984−6003.
(46) Palacios, A., Garcia, P., Padro, D., Lopez-Hernandez, E., Martin, I., and Blanco, F. J. (2006) Solution structure and NMR characterization of the binding to methylated histone tails of the plant homeodomain finger of the tumour suppressor ING4. *FEBS Lett. 580*, 6903−6908.
(47) Bernadó, P., Blanchard, L., Timmins, P., Marion, D., Ruigrok, R. W., and Blackledge, M. (2005) A structural model for unfolded proteins from residual dipolar couplings and small-angle x-ray scattering. *Proc. Natl. Acad. Sci. U. S. A. 102*, 17002−17007.
(48) Ozenne, V., Bauer, F., Salmon, L., Huang, J. R., Jensen, M. R., Segard, S., Bernado, P., Charavay, C., and Blackledge, M. (2012) Flexible-meccano: a tool for the generation of explicit ensemble descriptions of intrinsically disordered proteins and their associated experimental observables. *Bioinformatics 28*, 1463−1470.
(49) Eyal, E., Najmanovich, R., McConkey, B. J., Edelman, M., and Sobolev, V. (2004) Importance of solvent accessibility and contact surfaces in modeling side-chain conformations in proteins. *J. Comput. Chem. 25*, 712−724.
(50) Hess, B., Kutzner, C., van der Spoel, D., and Lindahl, E. (2008) GROMACS 4: Algorithms for Highly Efficient, Load-Balanced, and Scalable Molecular Simulation. *J. Chem. Theory Comput. 4* (3), 435−47.
(51) Lindorff-Larsen, K., Piana, S., Palmo, K., Maragakis, P., Klepeis, J. L., Dror, R. O., and Shaw, D. E. (2010) Improved side-chain torsion potentials for the Amber ff99SB protein force field. *Proteins 78*, 1950−1958.
(52) Jorgensen, W. L., Chandrasekhar, J., Madura, J. D., Impey, R. W., and Klein, M. L. (1983) Comparison of simple potential functions for simulating liquid water. *J. Chem. Phys. 79*, 926.
(53) Rambo, R. P. *ScÅtter, a JAVA-based application for basic analysis of SAXS datasets, Version 3.1R*; Diamond Light Source: Didcot, U.K., 2017.
(54) Svergun, D. I. (1992) Determination of the regularization parameter in indirect-transform methods using perceptual criteria. *J. Appl. Crystallogr. 25*, 495−503.
(55) Svergun, D. I., Barberato, C., and Koch, M. H. J. (1995) CRYSOL - a Program to Evaluate X-ray Solution Scattering of Biological Macromolecules from Atomic Coordinates. *J. Appl. Crystallogr. 28*, 768−773.
(56) Palacios, A., Munoz, I. G., Pantoja-Uceda, D., Marcaida, M. J., Torres, D., Martin-Garcia, J. M., Luque, I., Montoya, G., and Blanco, F. J. (2008) Molecular basis of histone H3K4me3 recognition by ING4. *J. Biol. Chem. 283*, 15956−15964.
(57) Jimenji, T., Matsumura, R., Kori, S., and Arita, K. (2019) Structure of PCNA in complex with DNMT1 PIP box reveals the basis for the molecular mechanism of the interaction. *Biochem. Biophys. Res. Commun. 516*, 578−583.

DOI: 10.1021/acschembio.9b00679
ACS Chem. Biol. 2019, 14, 2315−2326